A MILLION-MICROCHANNEL MULTIFUEL STEAM REFORMER FOR HYDROGEN PRODUCTION

Núria J. Divins[a,b,*], Trifon Trifonov[b], Ángel Rodríguez[c], Jordi Llorca[a,b,d,*]

[a]Institute of Energy Technologies, Universitat Politècnica de Catalunya, Campus EEBE, Av. Eduard Maristany 16, 08019 Barcelona, Spain.

[b]Barcelona Research Centre in Multiscale Science and Engineering, Universitat Politècnica de Catalunya, Campus EEBE, Av. Eduard Maristany 16, 08019 Barcelona, Spain.

[c]Department of Electronic Engineering, Universitat Politècnica de Catalunya, Campus Nord, c/ Jordi Girona 1-3, 08034 Barcelona, Spain.

[d]Department of Chemical Engineering, Universitat Politècnica de Catalunya, Campus EEBE, Av. Eduard Maristany 16, 08019 Barcelona, Spain.

*Corresponding authors

Núria J. Divins, Jordi Llorca

e-mail: nuria.jimenez.divins@upc.edu

Tel.: (+34) 93 4010701

Abstract

A functionalized silicon micromonolith of 7 mm in diameter and 210 µm-thick was evaluated for the production of hydrogen from the steam reforming (SR) of various fuels, containing different functional groups, such as ethanol, acetic acid, 2-propanol, acetone, and 2-methoxyethanol. The micromonolith consisted of 2 million regular channels of 3.3 µm in diameter, which were coated with a 100-nm $RhPd/CeO_2$ catalytic layer. The catalytic activity was tested at temperatures between 823-1023 K, using overstoichiometric steam-to-carbon ratios and operating at contact times between 0.005-0.009 s. The best performance was obtained for the 2-methoxyethanol SR tests, where 53% H_2 selectivity was recorded. A remarkable hydrogen production normalized by reactor volume of 110 $L_N H_2 \cdot mL_{2\text{-methoxyethanol,liquid}}^{-1} \cdot cm^{-3}_{Reactor}$ was recorded, leading to comparable H_2 yields to those obtained with a conventional monolith coated with the same $RhPd/CeO_2$ catalyst, owing to the large contact area. After more than 80 hours under reaction conditions, the micromonolith was characterized by SEM and TEM. SEM analyses showed that no channels were blocked due to carbon deposition nor detached CeO_2 layers were found. These results demonstrate the feasibility of using catalytic Si micromonoliths as microreformers to generate hydrogen from the SR of different fuels to power portable fuel cells.

Keywords: microreactor, multifuel, silicon micromonolith, hydrogen, steam reforming (SR), $RhPd/CeO_2$ catalyst.

1. Introduction

In the last two decades, much attention has been directed towards microreactor technology and, in particular, in the field of energy technology [1,2]. The intrinsic properties of microstructured reactors, which are composed of channels in the micrometer range, offer superior heat and mass transfer properties than conventional reactors with larger volumes, as well as safe, compact, and modular operation, thus allowing for process intensification [3]. These properties make microreactors attractive for thermochemical conversion and, in this regard, several groups have developed microscale reformers, i.e. microreformers, to convert hydrocarbons, alcohols or ammonia to hydrogen-rich streams that can be coupled to low-temperature fuel cells (FC), i.e. polymer electrolyte membrane (PEM) FC, or solid oxide FC [4]. Microreformers enable the on-site and/or on-demand hydrogen production to feed FC, thus being a practical alternative to hydrogen storage [5], avoiding the difficulties it imposes. Therefore, microreactors appear as a valuable technology to power portable and mobile devices, spanning from several kW to less than 100 W [1].

Several factors affect microreactor design, such as fuel cell type, fuel type, fuel processing approach, operating temperature, catalyst, reactor architecture and materials of fabrication [4]. Considering the miniaturization trend of FC systems, developing microreformers where the hydrogen production scale follows this miniaturization is needed. Meeting these needs requires developing novel manufacturing techniques that allow increasing the hydrogen production per reactor volume while maintaining the system efficiency. In this regard, we have achieved this by using silicon wafers where millions of cylindrical and parallel channels of only 2-4 μm in diameter and ca. 200 μm-long are produced by photo-assisted electrochemical etching [6]. The resulting micromonoliths contain an outstanding number of 4 million channels per square centimeter arranged in a square matrix. This geometry leads to a dramatic increase of the geometric surface area exposed to reactants per reactor volume in the range of 10^5-10^6 m^2/m^3, which is two orders

of magnitude higher than for conventional monoliths. Moreover, the regular distribution of channels assures a homogeneous flow distribution. Besides, the use of macroporous silicon allows for its integration with FC on Si technology [7].

A tremendous amount of studies have been reported using microreactors to produce hydrogen from the steam reforming (SR) of different fuels, being methanol, methane, ethanol, and butane the most widely researched [4]. Nevertheless, the hydrogen production from the SR of other renewable substrates, such as polyalcohols, has arisen as a promising route [8,9]. In our previous studies, catalytic silicon micromonoliths had shown an excellent performance to produce hydrogen from the SR of ethanol and dimethyl ether [6,10,11], where H_2 production rates normalized per reactor volume two orders of magnitude higher than in conventional reactors were achieved, and to purify hydrogen by selectively oxidizing CO from H_2/CO/air streams [12]. In this work, we extend these studies by testing the feasibility and stability of functionalized Si micromonoliths to reform different types of fuels and withstand severe reaction conditions (temperatures up to 1023 K) since, as mentioned above, these are key factors affecting microreactor design. To that end, we investigated the generation of hydrogen from the SR of relevant model organic compounds containing different functional groups and longer carbon chains, namely, alcohols, acids, ethers, ketones, and hydrocarbons. In particular, ethanol, acetic acid, propanone (acetone), 2-propanol (isopropanol), 2-methoxyethanol (methyl cellosolve, $C_3H_8O_2$) and a diesel surrogate (equivalent formula $C_{12}H_{23}$) were chosen [13,14]. The suitability of these compounds to generate hydrogen from their steam reforming reactions has been previously investigated in conventional reactors. Acetic acid is a model compound of an organic acid and it is the most representative compound of bio-oil, whose concentration can be up to 12%. Ketones present in bio-oil can be represented by acetone, whose concentration can reach up to 2.8% [15]. On the other hand, the semiconductor industry generates large quantities of waste solutions, which are often composed of aqueous mixtures containing ethanol, isopropanol,

acetone, 1-methoxy-2-propanol and butanone and, thus, their SR has been proposed as a suitable alternative to revalorize this waste by producing H_2 [16]. In the literature, rhodium-based catalysts have been commonly chosen to reform some of the above-mentioned compounds, and, among the various supports tested, CeO_2-supported Rh catalysts showed to be resistant to coke formation [17,18]. In this regard, a catalyst composed of RhPd nanoparticles supported on CeO_2 was selected for this study due to its high ability to break C-C bonds, high H_2 selectivity, long stability and low C deposition [19,20].

2. Experimental Methods

2.1. Silicon micromonoliths fabrication

The fabrication process of the silicon micromonoliths has been described elsewhere [21,22]. The structured supports were manufactured by photoelectrochemically etching n-type, float-zone (100) silicon wafers with a resistivity of 2-6 Ω·cm. Prior to the electrochemical etching, lithography was used to pre-structure the wafer surface creating a squared matrix of 4-µm pitch. Subsequently, etching with tetramethylammonium hydroxide (TMAH) was performed to create a squared array of inverted pyramids pointing towards the bulk of the wafer. These pyramids defined the positions of pore growth. Next, the electrochemical etching was performed at 288 K bringing the pre-structured surface in contact with an electrolyte composed of 5 wt.% hydrofluoric acid (HF) solution and TritonX-100 surfactant (0.1 mmol) as a wetting agent, while the back side was illuminated using LEDs with an 880-nm peak emission wavelength. A constant anodic potential of 2 V was applied for ca. 330 min to achieve a pore depth of 210 µm. After the photoelectrochemical etching, oxidation with dry O_2 at 1373 K for 30 min was carried out to grow a SiO_2 layer on the microchannels' walls and the front side. To open the channels from the reverse side, a 25 wt.% TMAH solution at 358 K was used to etch off the remaining Si. The process ended

dipping the samples in 5 wt.% HF to remove the remaining oxides. The fabrication procedure leads to silicon micromonoliths 210 µm-thick and 13 mm in diameter, as seen in Figures 1a and 1b, containing ca. $4 \cdot 10^6$ microchannels·cm^{-2} of 3.3 µm in diameter, perfectly regular, opened at both sides and arranged in a square lattice with 4 µm periodicity (Figure 1c). This results in a geometric surface-area-to-volume ratio of $1.2 \cdot 10^6$ m^2m^{-3} and an open frontal area of 34%. The pressure drop of the micromonolith was characterized by flowing nitrogen at room temperature and, for instance, a pressure drop of only 102 Pa was measured flowing 37 $mLmin^{-1}$, which is in good agreement with the corresponding value obtained with the Poiseuille law [23].

2.2. Catalytic coatings development

After the fabrication process, the Si micromonolith was oxidized with dry O_2 at 1373 K for 30 min to develop a SiO_2 layer over the walls of the microchannels. Subsequently, cerium 2-methoxyethoxide (liquid, Alfa Aesar) was forced to pass through the channels by applying a pressure gradient of 75 kPa between both sides of the micromonolith by using a vacuum pump. Next, the micromonolith with filled channels was calcined at 773 K for 6 h (5 $Kmin^{-1}$) to decompose the cerium precursor and form a CeO_2 layer on top of the SiO_2 layer (Figure 2). Subsequently, nominal 0.5 wt.% Rh and 0.5 wt.% Pd were anchored on the CeO_2 layer by passing a $PdCl_2$+$RhCl_3$ (Sigma Aldrich) water/acetone solution through the coated microchannels (free impregnation). Finally, the catalytic micromonolith was dried at 393 K overnight and calcined in air at 573 K for 6 h (2 $Kmin^{-1}$).

2.3. Materials characterization

Powder X-ray diffraction (XRD) was performed using a Bruker D8 Advance (Bruker, Germany) diffractometer equipped with Ni-filtered (2 μm thickness) Cu Kα radiation and operating at 40 kV and 40 mA (acquisition range from 10º to 80º, 0.02º step size and 1s dwell time). High-resolution transmission electron microscopy (HRTEM) images were obtained at 200 kV with a JEOL JEM-2010F equipped with a field emission gun. Scanning electron microscopy (SEM) images were acquired with a Neon40 crossbeam station equipped with a Schottky field emission gun (Carl Zeiss) operated at 5 keV and a focused Ga^+ ion beam (FIB) (CANION31, Orsay).

2.4. Catalytic tests

The functionalized Si micromonolith was cut with a laser forming a disk of 8 mm in diameter and glued with epoxy to a stainless steel washer (outer diameter (OD) 19 mm; inner diameter (ID) 7 mm), leaving $1.5 \cdot 10^6$ microchannels exposed to reactants. This was subsequently sealed inside a stainless steel reactor that was placed inside a tubular furnace (Carbolite) for catalytic testing. Fuel/water mixtures were dosed with a syringe pump (Kent Scientific), which were evaporated before reaching the microreactor with heating bands. The fuels tested were synthetic ethanol (Panreac), acetic acid (Panreac), acetone (Scharlau), isopropanol (Fisher Scientific), 2-methoxyethanol (Acros Organics) and a diesel surrogate of equivalent formula $C_{12}H_{23}$ (Repsol). To avoid the formation of carbonaceous deposits, overstoichiometric water/fuel ratios were tested [1]. For ethanol and acetic acid steam reforming tests, the water/fuel ratio was kept at 6 and for the other fuels, which are composed of longer C chains, the ratio was increased up to 15, to prevent the deactivation of the catalyst due to coke deposition. The corresponding S/C ratios are listed in Table 1.

Table 1. Steam-to-carbon ratios and gaseous streams used for the different tests.

Reforming reaction	S/C	Fuel (mol_{gas}/min)	Steam (mol_{gas}/min)
Ethanol SR (eq. 1)	3	$1.1 \cdot 10^{-4}$	$6.9 \cdot 10^{-4}$
Acetic acid SR (eq. 2)	3	$1.2 \cdot 10^{-4}$	$6.9 \cdot 10^{-4}$
Acetone SR (eq. 3)	5	$5.5 \cdot 10^{-5}$	$8.3 \cdot 10^{-4}$
Isopropanol SR (eq. 4)	5	$5.5 \cdot 10^{-5}$	$8.2 \cdot 10^{-4}$
2-Methoxyethanol SR (eq. 5)	5	$5.4 \cdot 10^{-4}$	$8.2 \cdot 10^{-4}$
Diesel surrogate SR (eq. 6)	6.8	$1.0 \cdot 10^{-5}$	$8.3 \cdot 10^{-4}$

Prior to each reforming test, the catalyst was reduced in a 10% H_2/He mixture (50 $mLmin^{-1}$ total) at 623 K (5 $Kmin^{-1}$) for 1 h, which was dosed using mass flow controllers (M+W instruments). The reforming tests were performed at atmospheric pressure, temperatures ranging between 823 K and 1023 K and at a fixed injection rate of liquid reactants mixture (0.019 $mLmin^{-1}$). 10 $mLmin^{-1}$ of N_2 were added at the inlet and were used as an internal standard. These reaction conditions represented contact times of $5\text{-}9 \cdot 10^{-3}$ s. No regeneration treatments were performed between the different reforming tests. The condensable products from the reactor effluent were collected in a condenser and the gaseous effluent was analyzed online under steady-state conditions with a microchromatograph (μGC) (Agilent 3000A), which was equipped with a 5 Å Molsieve, a PLOT U and a Stabilwax column. Outlet molar flowrates of the non-condensable products (H_2, CO, CO_2, CH_4) of the reactor effluent were calculated using the composition obtained from the chromatographic analyses and total volumetric flowrate data.

The steam reforming reactions (including the water-gas shift reaction) of the different compounds investigated are listed in equations 1-6.

Ethanol SR: $CH_3CH_2OH + 3H_2O \longrightarrow 6H_2 + 2CO_2$ (1)

Acetic acid SR: $CH_3COOH + 2H_2O \longrightarrow 4H_2 + 2CO_2$ (2)

Acetone SR: $CH_3COCH_3 + 5H_2O \longrightarrow 8H_2 + 3CO_2$ (3)

Isopropanol SR: $CH_3CHOHCH_3 + 5H_2O \longrightarrow 9H_2 + 3CO_2$ (4)

2-Methoxyethanol SR: $CH_3OCH_2CH_2OH + 4H_2O \longrightarrow 8H_2 + 3CO_2$ (5)

Diesel surrogate SR: $C_{12}H_{23} + 24H_2O \longrightarrow 35.5H_2 + 12CO_2$ (6)

The SR of these fuels yields a different maximum number, x, of H_2 moles, per mole of fuel reacted. Therefore, to compare the performance of the catalytic micromonolith for the different fuels, this factor was taken into consideration to normalize the H_2 yield of each experiment, leading to H_2 yields defined between 0 and 1, as presented in equation 7. The selectivity to reaction products was calculated according to equation 8.

$$\theta_{H_2} = \frac{\dot{n}_{H_2}}{x\,\dot{n}_{fuel}} 100 \quad , \quad \text{n=moles} \tag{7}$$

$$S_i = \frac{\dot{n}_i}{\sum_i \dot{n}_i} 100, \qquad \text{i=}H_2, CO_2, CH_4, CO, \ldots \tag{8}$$

3. Results and discussion

3.1. Functionalization of the silicon micromonolith

The small dimensions of the microchannels and their large aspect ratio (depth/diameter>65) required developing a new route to coat the walls of the microchannels with thin catalytic layers without blocking them, as reported elsewhere [6,10–12]. Specifically, the functionalization process consisted of an initial oxidation at 1373 K for 30 min of the Si micromonolith, leading to the formation of homogeneous SiO_2 layers ca. 100-nm thick, as seen in Figure 2. The hydroxyl

groups present on the SiO_2 layer served as anchoring sites for the liquid cerium alkoxide (Ce(O-CH_2-CH_2-O-CH_3)$_4$) precursor. After calcination of cerium methoxyethoxide at 773 K, 100-nm thick CeO_2 layers were developed on the grown SiO_2 layers. Figure 2 shows SEM images corresponding to an as-functionalized Si micromonolith, where a cross-sectional cut had been performed for characterization purposes. Rh and Pd nanoparticles (NPs) were subsequently anchored to the CeO_2 layers via free impregnation followed by calcination at 573 K for 6 h. Some metal aggregates correspond to the bright dots visible inside the channel in Figure 2a. Figure 2b shows two adjacent channels with the detail of the catalytic coatings developed on the Si micromonolith structure: the Si wall is visible at the center, covered by uniform and well-adhered SiO_2 layers of ca. 100 nm thickness (dark grey), which are completely coated with homogeneous and well-anchored 100-nm thick CeO_2 layers (light grey). The crystalline structure of the developed coating was studied by XRD. The diffractograms revealed peaks at interplanar distances (d_{hkl}) of 3.1, 2.7, 1.9 and 1.6 Å, which correspond to the interplanar distances of CeO_2 fcc, thus confirming that the desired CeO_2 structure was formed. This characterization proves that the method developed leads to thin catalytic layers of CeO_2-based catalysts and, thus, to the successful functionalization of Si micromonoliths. Taking into account that the channels measure 3.3 µm in diameter and that the catalytic coatings are 0.1-µm thick, this results in an exposed geometric area per reactor volume of $1.4 \cdot 10^6$ m^2m^{-3}.

3.2. Catalytic tests

3.2.1. Steam reforming tests

Initially, ethanol SR tests without dilution (i.e., without adding N_2 to the reactants feed) were carried out to assure the correct performance of the catalytic micromonolith. The ethanol SR tests were carried out at 923 K. The selectivity towards reforming products was 48% H_2, 16% CH_4, 21%

CO and 5% CO_2; together with less than 5% CH_3CHO and C_2 products, which is similar to the values reported previously [10].

Next, the steam reforming tests with the fuels described above were performed (reactions 2 to 6) at temperatures between 823 and 1023 K (except for acetic acid, for which the maximum reaction temperature was 973 K). For these tests, N_2 was used as an internal standard, as described in section 2.4. Figure 3a shows the hydrogen yield obtained for the acetic acid, acetone, isopropanol and 2-methoxyethanol SR tests for the whole range of temperatures studied. The equilibrium values corresponding to 923 K are listed in table 2.

Table 2. Equilibrium values on a dry basis at 923 K for the SR of different fuels.

Reforming fuel	**H_2 (%)**	**CO (%)**	**CH_4 (%)**	**CO_2 (%)**
Acetic acid	65.0	23.1	0.7	11.2
Acetone	74.4	2.3	0.0	23.2
Isopropanol	60.1	11.9	0.7	27.4
2-methoxyethanol	70.1	4.7	0.0	25.2

As seen in Figure 3a, for the acetic acid, acetone, and isopropanol SR tests, the hydrogen yield increased as the reaction temperature increased, indicating that the H_2 production was promoted at higher reaction temperatures (see also Figure S1, Supplementary Materials). A different trend was observed for the 2-methoxyethanol SR tests, for which the θ_{H_2} decreased at 973 K. As seen in the selectivity trend (Figure S1), the CO concentration increased and that of CO_2 decreased as the reaction temperature increased. This indicates that the water-gas shift (WGS) reaction ($CO + H_2O \leftrightarrows CO_2 + H_2$) proceeded to a lesser extent at higher temperatures, as expected [1], resulting in a decrease of the H_2 selectivity. For all temperatures, the hydrogen yield obtained with the microreformer followed the trend acetone < isopropanol < acetic acid < 2-methoxyethanol.

Figure 3b reports the selectivity towards H_2, CH_4, CO, CO_2, and other byproducts detected described below, categorized as *others*, at 923 K, which is an intermediate temperature for SR tests. The selectivity for the other reaction temperatures tested is shown in Figure S1. During the acetic acid SR tests, H_2, CO_2, CO, and CH_4 were the only reaction products detected. At 923 K, the acetic acid SR rendered 29% H_2 selectivity (Figure 3b). On the other hand, for the acetone SR tests, mainly acetone was detected, indicating a low activity of the catalyst for the acetone SR and the other byproducts detected were C_2H_4 and C_2H_6. The H_2 selectivity increased significantly during the isopropanol SR tests, up to 53% at 923 K. At this temperature, up to 23% of acetone was produced together with CO, CH_4, and CO_2, which suggests that along with the isopropanol SR reaction, isopropanol dehydrogenation and CO methanation were taking place as well [14,18]. These selectivity values are in line with previously reported results for Rh-based catalysts [18]. For the SR of 2-methoxyethanol at 923 K, the H_2 selectivity reached 53% and concentrations below 1% of C_2H_4, CH_3CHO and C_2H_6 were detected. Among the different fuels tested, the highest hydrogen yield, θ_{H_2}=0.4, was attained from 2-methoxyethanol SR. Probably, the absence of C-C bonds in the methoxy group facilitates the reforming process, resulting in higher H_2 productions. At the end of the experiments with the different fuels reported above, a diesel surrogate SR test at 1023 K was also performed. Nevertheless, very low activity and hydrogen yield were attained (<0.01). The whole series of experiments described above represented ca. 80 hours of operation.

Comparing the equilibrium values reported in Table 2 and the selectivity values achieved for the different fuels tested, under the operational conditions applied in this study, the equilibrium was not reached. This is ascribed to the short contact times achieved in the microreformer, which can be remediated by stacking of microreformer units (numbering up). This is a common strategy in microreactor technology.

3.2.2. Performance comparison with conventional monoliths

The best catalytic performance of the catalytic Si micromonolith, which was attained for the 2-methoxyethanol SR tests, was compared with that of conventional reactors. To that end, the hydrogen production density (hydrogen production normalized by reactor volume) per mole of 2-methoxyethanol fed [$mL_{H_2,gas}/(mL_{fuel,liquid} \cdot cm^3_{Reactor})$] was calculated. Taking into account the volume of the micromonolith disk, the 2-methoxyethanol SR tests at 923 K, rendered an outstanding H_2 production density of 110 $L_N H_2/(mL_{2\text{-methoxyethanol,liquid}}\ cm^3_{Reactor})$ at contact times of only 5.7 ms, which corresponds to a spatial velocity of $6.3 \cdot 10^6\ h^{-1}$. If the production density is multiplied by the reactor volume, a value of 0.90 $L_N H_2/mL_{2\text{-methoxyethanol,liquid}}$ is obtained. Comparing this value with that obtained for the 2-methoxyethanol SR on a 400 cells per square inch (cpsi) cordierite monolith functionalized with the same $RhPd/CeO_2$ catalyst (T=923 K, S/C=3, GHSV=$10^2\ h^{-1}$, atmospheric pressure) (results reported in [13]) a similar value of 0.99 $L_N H_2/mL_{2\text{-methoxyethanol,liquid}}$ was achieved. Remarkably, despite the three orders of magnitude difference between the dimensions of the channels of the Si micromonolith and of a conventional cordierite monolith, resulting in operational spatial velocities 4 orders of magnitude higher for the Si micromonoliths, similar H_2 productions per mole of fuel fed were attained. The unique geometry of the Si micromonoliths with channels of only 3.3 µm leads to a remarkable surface-area-to-volume ratio of $1.4 \cdot 10^6\ m^2m^{-3}$ vs. $2.2 \cdot 10^3\ m^2m^{-3}$ for a 400 cpsi monolith, which allows obtaining similar hydrogen yields despite the enormous increase of the spatial velocity.

3.3. Characterization of the catalytic silicon micromonolith after the reaction tests

After the SR tests, the Si micromonolith was disassembled from the reactor housing and a cross-sectional cut was performed to investigate the catalytic coatings by SEM. Figure 4a shows the detail of four consecutive channels after the reaction tests. The severe reaction conditions tested during the steam reforming of the different fuels, including diesel, caused changes on the ceria

coating as well as the formation of some carbonaceous deposits. Nevertheless, despite the aggressive reaction conditions applied, no channels blocked by carbon deposition nor detached CeO_2 layers were detected. A detail of the inside of one microchannel is shown in Figure 4b, where a well-developed and homogeneous CeO_2 layer flawlessly anchored to the SiO_2 layer is seen. To get insight into the catalyst structure after the reaction tests by HRTEM, a lamella was fabricated from the reacted microchannels with a SEM-FIB. First, the region of interest was covered with a thin Pt layer (~200 nm) to protect it from the ion beam damage (Figure 4d). With the FIB, ca. 80 µm-deep grooves were performed on the front and the back side of the Pt strip by milling the microchannels at different depths with Ga^+ ions (current 30 kV, 10 nA) (Figures 4d,e,f). Then, by finer milling (30 kV, 2 nA) an isolated and intact part was left, which was thinned down until a piece of about one microchannel thickness and four microchannels depth was obtained. Next, a micromanipulator with a tungsten tip was attached to one side of the Pt strip by Pt deposition (Figure 4g). Subsequently, the opposite side of the Pt strip was cut and the micromanipulator attached to the isolated lamella was lifted out. The sample was then attached to a TEM sample holder by Pt deposition and the microchannels were polished until they were thin enough to be transparent to electrons (60 to 70 nm thickness), allowing the performance of TEM measurements (Figure 4h). After this process, the lamella was removed from the SEM system and it was examined by TEM.

HRTEM analyses revealed dispersed RhPd NPs over the CeO_2 support, as seen in Figure 5. Remarkably, after the exposure to reforming conditions of different fuels at temperatures between 823 and 1023 K and the lamella fabrication process, most of the RhPd NPs identified were in close contact with the CeO_2 support. The HRTEM images show that the NPs underwent moderate sintering, as the NP size after the reaction tests was 7±2 nm (before reaction the NPs measured ca. 3 nm, see [19]) and were still alloyed. In Figure 5a, small disseminated NPs around the sample were ascribed to Pt NPs deposited during Pt deposition carried out during the lamella fabrication

process, since they are homogeneously distributed over the sample, including the CeO_2 and SiO_2 layers and are smaller than RhPd NPs, as they measure ca. 2 nm. Therefore, the fabrication of the lamella allowed for the characterization of catalytic layers, which constituted the active phase of a real microreactor exposed to severe working conditions (high temperature and large steam content) for ca. 80 hours with stable operation.

4. Conclusions

The feasibility and suitability of using silicon micromonoliths to generate hydrogen from the steam reforming (SR) of various fuels containing different functional groups to power portable fuel cells were investigated. The microreformer consisted of a Si micromonolith of 7 mm in diameter containing ca. $1.5 \cdot 10^6$ channels of 3.3 µm in diameter, which was successfully functionalized with a $RhPd/CeO_2$ catalyst. The SR reaction tests proved the suitability of producing hydrogen from the SR of acetic acid, 2-propanol, and 2-methoxyethanol, and showed that the best performance was achieved with 2-methoxyethanol, where the highest hydrogen yield was recorded. Hydrogen production rates normalized by micromonolith volume of 110 $L_N H_2/(mL_{2\text{-methoxyethanol,liquid}}\ cm^3_{Reactor})$ at contact times of only 5.7 ms were reached. The three orders of magnitude increase in the geometric surface area per reactor volume in Si micromonoliths leads to production rates comparable to those obtained on conventional 400 cpsi ceramic monoliths, despite the reduction of the contact time four orders of magnitude. The advanced characterization by scanning and transmission electron microscopy of the micromonolith after reaction showed that no microchannels were blocked with carbon deposits, owing to a good performance of the $RhPd/CeO_2$ catalyst, nor detached catalytic layers.

Acknowledgements

This work has been funded by projects MICINN/FEDER RTI2018-093996-B-C31 and GC 2017 SGR 128. NJD is thankful for the support from a Beatriu de Pinós grant (2018-BP-00146). JL is a Serra Húnter Fellow and is grateful to the ICREA Academia program. We thank Mrs. Marina Armengol for her technical assistance.

References

[1] G. Kolb, Review: Microstructured reactors for distributed and renewable production of fuels and electrical energy, Chem. Eng. Process. Process Intensif. 65 (2013) 1–44. https://doi.org/10.1016/j.cep.2012.10.015.

[2] P.L. Suryawanshi, S.P. Gumfekar, B.A. Bhanvase, S.H. Sonawane, M.S. Pimplapure, A review on microreactors: Reactor fabrication, design, and cutting-edge applications, Chem. Eng. Sci. 189 (2018) 431–448. https://doi.org/10.1016/j.ces.2018.03.026.

[3] H.J. Venvik, J. Yang, Catalysis in microstructured reactors: Short review on small-scale syngas production and further conversion into methanol, DME and Fischer-Tropsch products, Catal. Today. 285 (2017) 135–146. https://doi.org/10.1016/j.cattod.2017.02.014.

[4] J.D. Holladay, Y. Wang, A review of recent advances in numerical simulations of microscale fuel processor for hydrogen production, J. Power Sources. 282 (2015) 602–621. https://doi.org/10.1016/j.jpowsour.2015.01.079.

[5] M.S. Herdem, M.Y. Sinaki, S. Farhad, F. Hamdullahpur, An overview of the methanol reforming process: Comparison of fuels, catalysts, reformers, and systems, Int. J. Energy Res. 43 (2019) 5076–5105. https://doi.org/10.1002/er.4440.

[6] J. Llorca, A. Casanovas, T. Trifonov, A. Rodriguez, R. Alcubilla, First use of macroporous silicon loaded with catalyst film for a chemical reaction: A microreformer for producing hydrogen from ethanol steam reforming, J. Catal. 255 (2008) 228–233. https://doi.org/10.1016/j.jcat.2008.02.006.

[7] D. Pla, M. Salleras, A. Morata, I. Garbayo, M. Gerbolés, N. Sabaté, N.J. Divins, A.

Casanovas, J. Llorca, A. Tarancón, Standalone ethanol micro-reformer integrated on silicon technology for onboard production of hydrogen-rich gas, Lab Chip. 16 (2016) 2900–2910. https://doi.org/10.1039/c6lc00583g.

[8] V. Shanmugam, R. Zapf, V. Hessel, H. Pennemann, G. Kolb, Nano-architectured CeO_2 supported Rh with remarkably enhanced catalytic activity for propylene glycol reforming reaction in microreactors, Appl. Catal. B Environ. 226 (2018) 403–411. https://doi.org/10.1016/j.apcatb.2017.12.062.

[9] A.E. Touri, M. Taghizadeh, Hydrogen Production via Glycerol Reforming over Pt/SiO_2 Nanocatalyst in a Spiral-Shaped Microchannel Reactor, Int. J. Chem. React. Eng. 14 (2016). https://doi.org/10.1515/ijcre-2015-0213.

[10] N.J. Divins, E. López, Á. Rodríguez, D. Vega, J. Llorca, Bio-ethanol steam reforming and autothermal reforming in 3-μm channels coated with $RhPd/CeO_2$ for hydrogen generation, Chem. Eng. Process. Process Intensif. 64 (2013) 31–37. https://doi.org/10.1016/j.cep.2012.10.018.

[11] C. Ledesma, E. López, T. Trifonov, Á. Rodríguez, J. Llorca, Catalytic reforming of dimethyl ether in microchannels, Catal. Today. 323 (2019) 209–215. https://doi.org/10.1016/j.cattod.2018.03.011.

[12] N.J. Divins, E. López, M. Roig, T. Trifonov, A. Rodríguez, F.G. de Rivera, L.I. Rodríguez, M. Seco, O. Rossell, J. Llorca, A million-channel CO-PrOx microreactor on a fingertip for fuel cell application, Chem. Eng. J. 167 (2011) 597–602. https://doi.org/10.1016/j.cej.2010.07.072.

[13] A. Hedayati, J. Llorca, Experimental study of 2-methoxyethanol steam reforming in a membrane reactor for pure hydrogen production, Fuel. 190 (2017) 312–317.

https://doi.org/10.1016/j.fuel.2016.11.004.

[14] C. Resini, L. Arrighi, M.C. Herrera Delgado, M.A. Larrubia Vargas, L. Alemany, P. Riani, S. Berardinelli, R. Marazza, G. Busca, Production of hydrogen by steam reforming of C3 organics over Pd–Cu/γγ-Al2O3 catalyst, Int. J. Hydrogen Energy. 31 (2006) 13–19. https://doi.org/10.1016/j.ijhydene.2005.04.014.

[15] A.A. Lemonidou, E.C. Vagia, Hydrogen production via steam reforming of bio-oil components over calcium aluminate supported nickel and noble metal catalysts, Appl. Catal. A Gen. 351 (2008) 111–121. https://doi.org/10.1016/j.apcata.2008.09.007.

[16] N. Palmeri, V. Chiodo, S. Freni, F. Frusteri, J.C.J. Bart, S. Cavallaro, Hydrogen from oxygenated solvents by steam reforming on Ni/Al2O3 catalyst, Int. J. Hydrogen Energy. 33 (2008) 6627–6634. https://doi.org/10.1016/j.ijhydene.2008.07.064.

[17] E.C. Vagia, A.A. Lemonidou, Investigations on the properties of ceria-zirconia-supported Ni and Rh catalysts and their performance in acetic acid steam reforming, J. Catal. 269 (2010) 388–396. https://doi.org/10.1016/j.jcat.2009.11.024.

[18] T. Mizuno, Y. Matsumura, T. Nakajima, S. Mishima, Effect of support on catalytic properties of Rh catalysts for steam reforming of 2-propanol, Int. J. Hydrogen Energy. 28 (2003) 1393–1399. https://doi.org/10.1016/S0360-3199(03)00042-9.

[19] E. López, N.J. Divins, A. Anzola, S. Schbib, D. Borio, J. Llorca, Ethanol steam reforming for hydrogen generation over structured catalysts, Int. J. Hydrogen Energy. 38 (2013) 4418–4428. https://doi.org/10.1016/j.ijhydene.2013.01.174.

[20] N.J. Divins, I. Angurell, C. Escudero, V. Pérez-Dieste, J. Llorca, Influence of the support on surface rearrangements of bimetallic nanoparticles in real catalysts, Science. 346 (2014) 620–623. https://doi.org/10.1126/science.1258106.

[21] V. Lehmann, The physics of macropore formation in low doped n-type silicon, J. Electrochem. Soc. 140 (1993) 2836–2843. https://doi.org/10.1149/1.2220919.

[22] T. Trifonov, M. Garín, A. Rodríguez, L.F. Marsal, R. Alcubilla, Tuning the shape of macroporous silicon, Phys. Status Solidi. 204 (2007) 3237–3242. https://doi.org/10.1002/pssa.200622537.

[23] S. Roy, R. Raju, H.F. Chuang, B.A. Cruden, M. Meyyappan, Modeling gas flow through microchannels and nanopores, J. Appl. Phys. 93 (2003) 4870. https://doi.org/10.1063/1.1559936.

Figure and figure legends

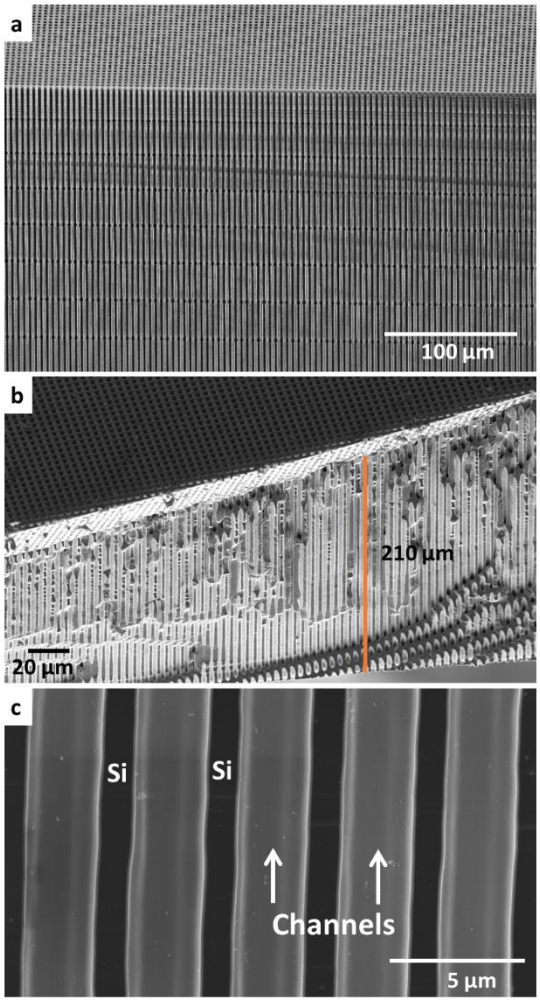

Figure 1. SEM images of the Si micromonolith used in this work. a) General view of the square array of regular microchannels. b) Cross-sectional cut of the Si micromonolith showing its thickness, which corresponds to the microchannels' length. c) Cross-sectional cut of the Si micromonolith showing the detail of five consecutive microchannels.

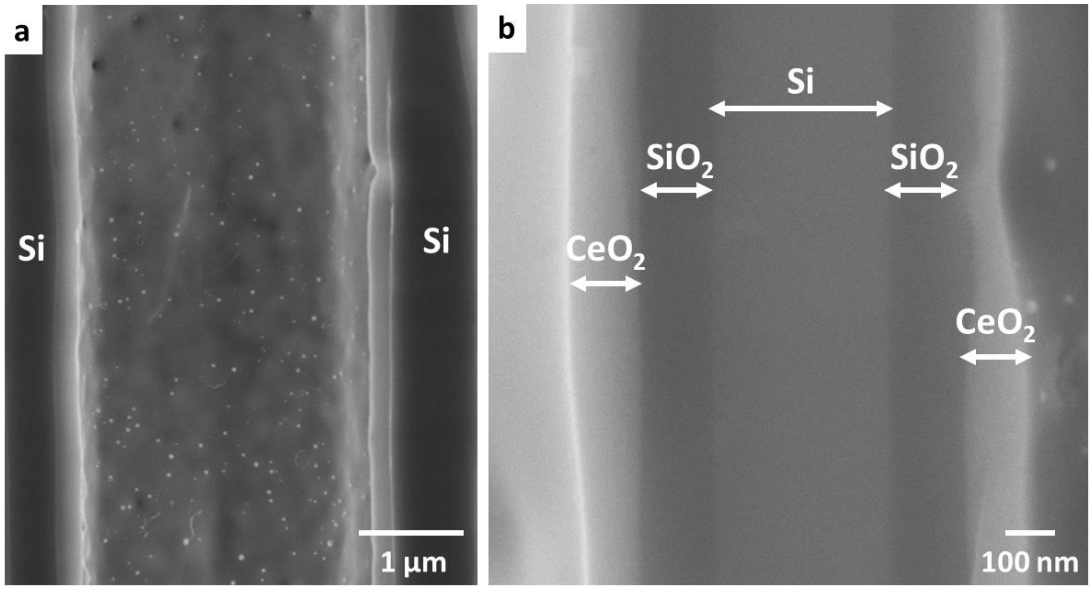

Figure 2. Representative SEM images of the functionalized Si micromonolith. a) Detail of the inner part of one channel showing the catalytic RhPd/CeO_2 coating deposited on a microchannel wall. b) Detail of a microchannel wall showing the catalytic coating developed on top: Si channel is visible at the center, the SiO_2 layers (dark grey) cover the Si wall, and the CeO_2 layers over the SiO_2 layers.

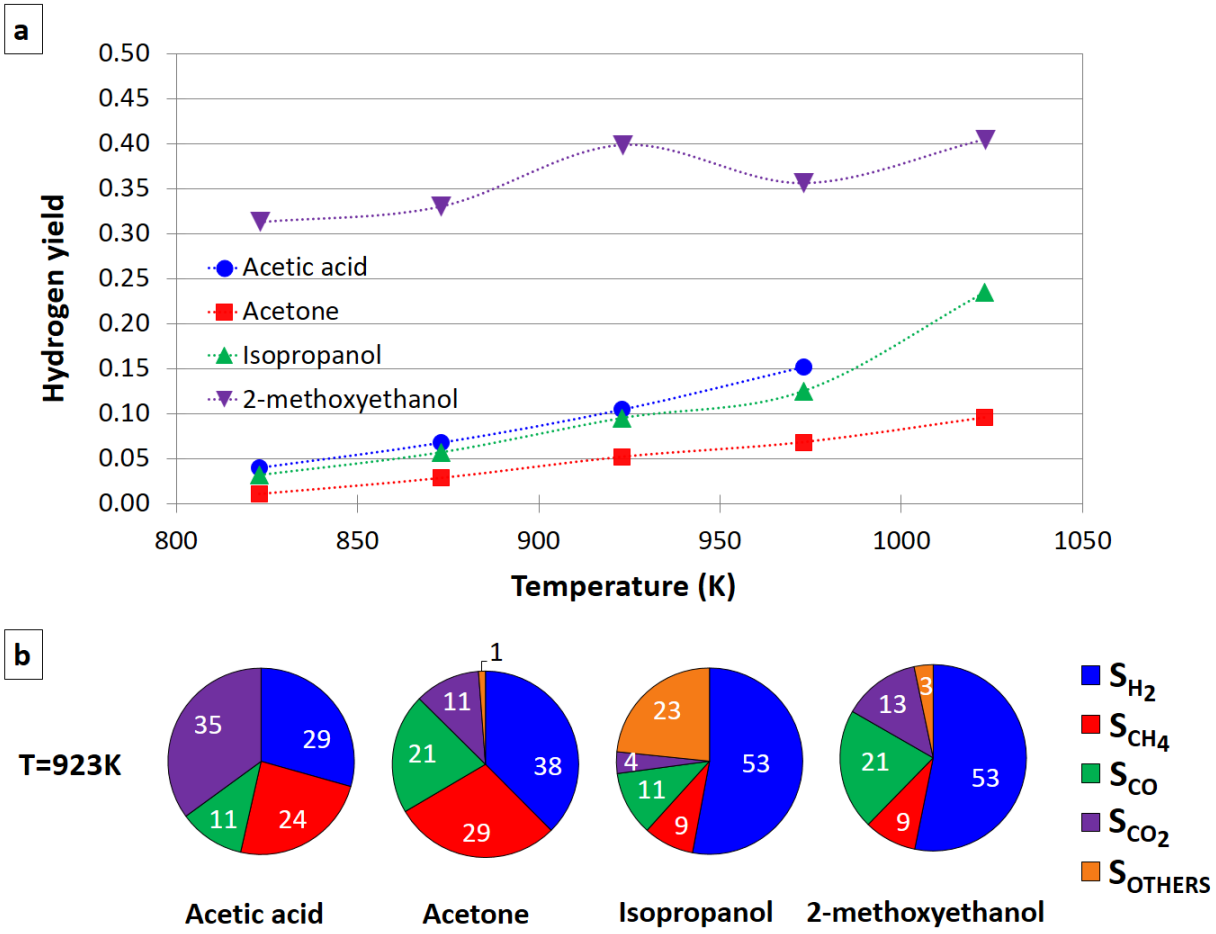

Figure 3. a) Hydrogen yield for the steam reforming tests of the indicated fuels. b) Selectivity obtained at 923 K. Tests carried out at P=1 bar, F=0.019 mL_{liquid} min^{-1}.

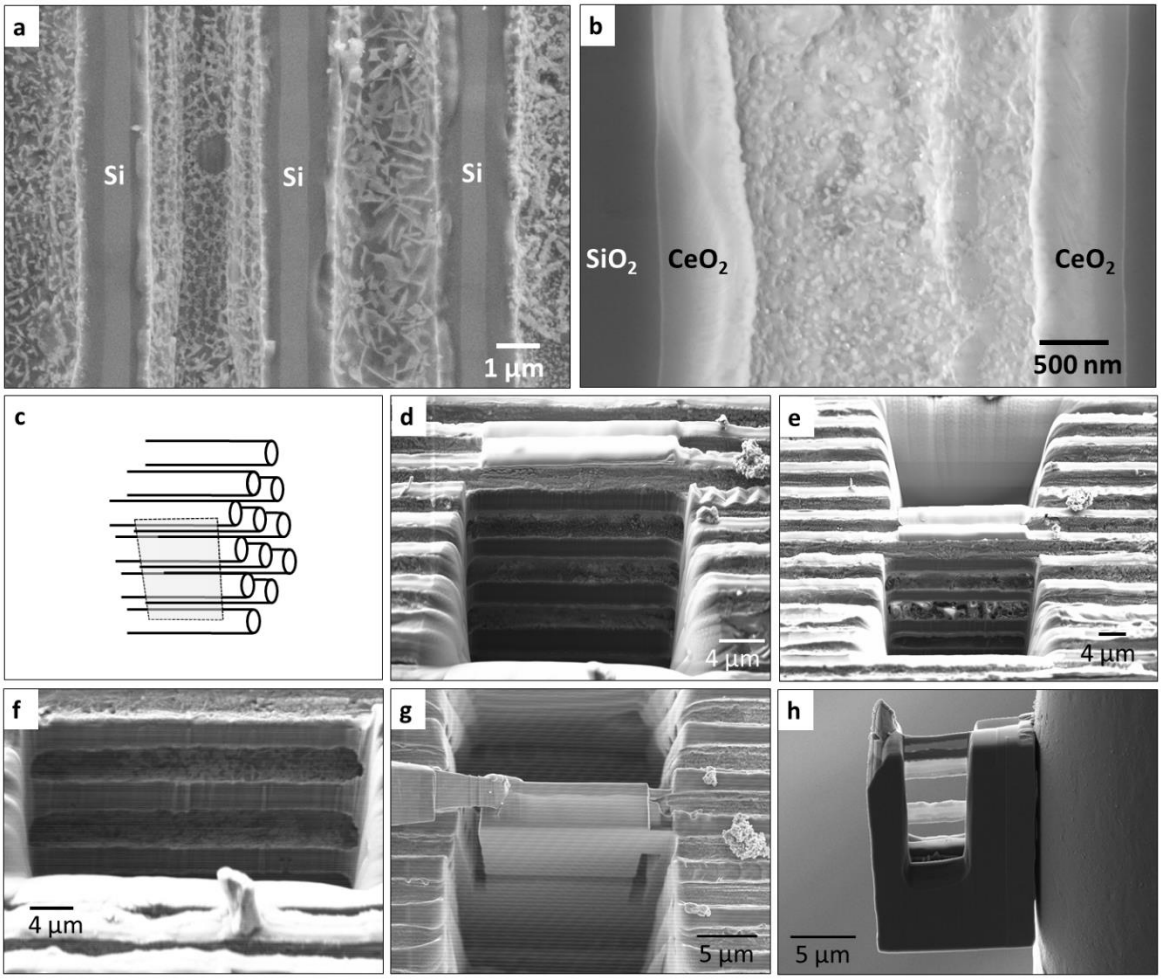

Figure 4. Representative SEM images of the functionalized micromonolith after 80 hours under reaction conditions. a) View of the post-reaction RhPd/CeO_2 coating inside the microchannels. b) Detail of one channel showing the CeO_2 layer covering the channel and attached to the SiO_2 layer. c) Schematic representation of the microchannels arrangement. d) to g) SEM images acquired chronologically during the fabrication process of a TEM lamella. d) to f) Detail of the catalytic layers inside the microchannels. g) Micromanipulator attached to isolated channels. h) Detail of the lamella attached to a TEM holder showing the detail of three microchannels polished and where the catalytic layers can be distinguished.

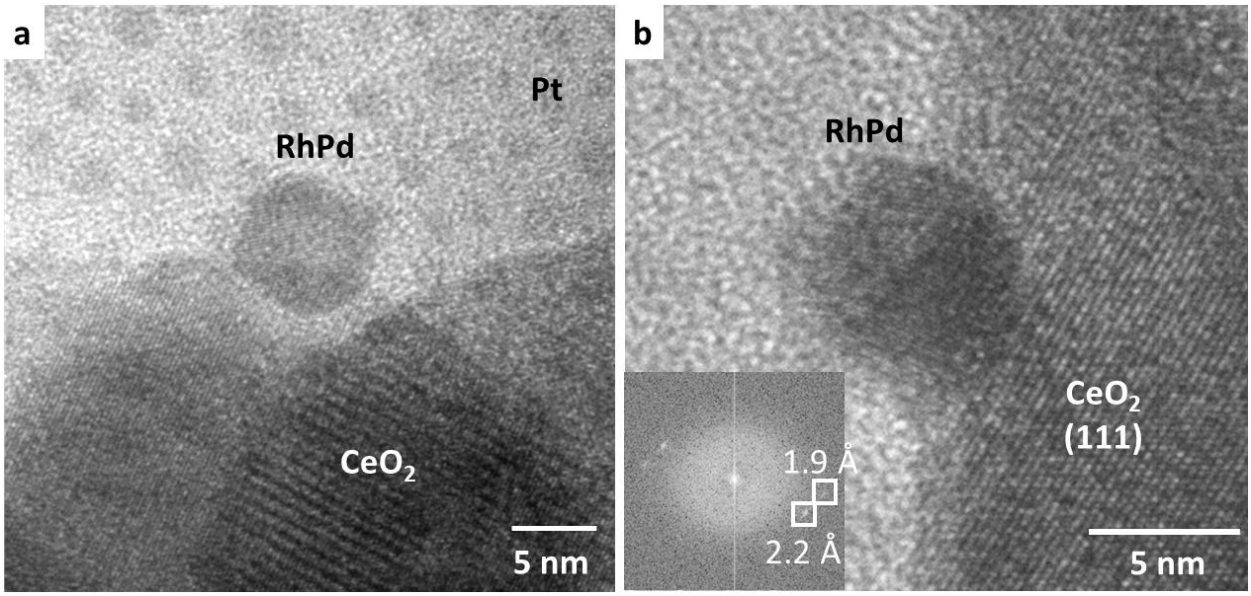

Figure 5. Representative HRTEM images of the RhPd/CeO_2 catalyst extracted from the Si micromonolith after the SR tests.